origin of the X_L, Y_L, Z_L coordinates. This cross point is also known as the goniometer centre or instrument centre.

Fig. 2.5.7(b) shows the relationship and stacking sequence among all rotation axes (ω, ψ, φ) and the sample coordinates S_1, S_2, S_3. ω is the base rotation; all other rotations and translations are on top of this rotation. The next rotation above ω is the ψ rotation. The next rotation above ω and ψ is the φ rotation. The sample coordinates S_1, S_2, S_3 are fixed to the sample regardless of the particular sample orientation given by the rotation angles (ω, ψ, φ). The φ rotation in the goniometer is intentionally chosen as a left-handed rotation so that the diffraction vectors will make a right-hand rotation observed in the sample coordinates S_1, S_2, S_3.

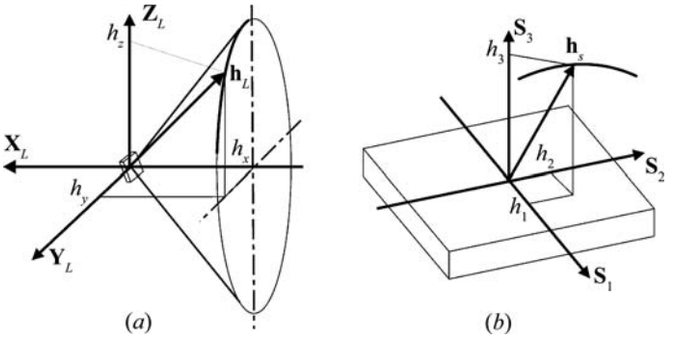

Figure 2.5.8
Unit diffraction vector in (a) the laboratory coordinates and (b) the sample coordinates.

2.5.2.4. *Diffraction-vector transformation*

2.5.2.4.1. *Diffraction unit vector in diffraction space and sample space*

In 2D-XRD data analysis, it is crucial to know the diffraction-vector distribution in terms of the sample coordinates S_1, S_2, S_3. However, the diffraction-vector distribution corresponding to the measured 2D data is always given in terms of the laboratory coordinates X_L, Y_L, Z_L because the diffraction space is fixed to the laboratory coordinates. Fig. 2.5.8 shows the unit vector of a diffraction vector in both (a) the laboratory coordinates X_L, Y_L, Z_L and (b) the sample coordinates S_1, S_2, S_3. In Fig. 2.5.8(a) the unit vector $\mathbf{h}_L$ is projected to the X_L, Y_L and Z_L axes as h_x, h_y and h_z, respectively. The three components are given by equation (2.5.5). In order to analyse the diffraction results relative to the sample orientation, it is necessary to transform the unit vector to the sample coordinates S_1, S_2, S_3. Fig. 2.5.8(b) shows the same unit vector, denoted by $\mathbf{h}_s$ projected to S_1, S_2 and S_3 as h_1, h_2 and h_3, respectively.

2.5.2.4.2. *Transformation from diffraction space to sample space*

The transformation of the unit diffraction vector from the laboratory coordinates X_L, Y_L, Z_L to the sample coordinates S_1, S_2, S_3 is given by

$$\mathbf{h}_s = \boldsymbol{A}\mathbf{h}_L, \tag{2.5.10}$$

where $\boldsymbol{A}$ is the transformation matrix. For Eulerian geometry in matrix form, we have

$$\begin{bmatrix} h_1 \\ h_2 \\ h_3 \end{bmatrix} = \begin{bmatrix} a_{11} & a_{12} & a_{13} \\ a_{21} & a_{22} & a_{23} \\ a_{31} & a_{32} & a_{33} \end{bmatrix} \begin{bmatrix} h_x \\ h_y \\ h_z \end{bmatrix}$$

$$= \begin{bmatrix} -\sin\omega\sin\psi\sin\varphi - \cos\omega\cos\varphi & \cos\omega\sin\psi\sin\varphi - \sin\omega\cos\varphi & -\cos\psi\sin\varphi \\ \sin\omega\sin\psi\cos\varphi - \cos\omega\sin\varphi & -\cos\omega\sin\psi\cos\varphi - \sin\omega\sin\varphi & \cos\psi\cos\varphi \\ -\sin\omega\cos\psi & \cos\omega\cos\psi & \sin\psi \end{bmatrix}$$

$$\times \begin{bmatrix} -\sin\theta \\ -\cos\theta\sin\gamma \\ -\cos\theta\cos\gamma \end{bmatrix}. \tag{2.5.11}$$

In expanded form:

$$\begin{aligned} h_1 &= \sin\theta(\sin\varphi\sin\psi\sin\omega + \cos\varphi\cos\omega) + \cos\theta\cos\gamma\sin\varphi\cos\psi \\ &\quad - \cos\theta\sin\gamma(\sin\varphi\sin\psi\cos\omega - \cos\varphi\sin\omega) \\ h_2 &= -\sin\theta(\cos\varphi\sin\psi\sin\omega - \sin\varphi\cos\omega) \\ &\quad - \cos\theta\cos\gamma\cos\varphi\cos\psi \\ &\quad + \cos\theta\sin\gamma(\cos\varphi\sin\psi\cos\omega + \sin\varphi\sin\omega) \\ h_3 &= \sin\theta\cos\psi\sin\omega - \cos\theta\sin\gamma\cos\psi\cos\omega - \cos\theta\cos\gamma\sin\psi \end{aligned} \tag{2.5.12}$$

In addition to the diffraction intensity and Bragg angle corresponding to each data point on the diffraction ring, the unit vector $\mathbf{h}_s\{h_1, h_2, h_3\}$ provides orientation information in the sample space. The transformation matrix of any other goniometer geometry, such as kappa geometry (Paciorek *et al.*, 1999), can be introduced into equation (2.5.10) so that the unit vector $\mathbf{h}_s\{h_1, h_2, h_3\}$ can be expressed in terms of the specified geometry. All equations using the unit vector $\mathbf{h}_s\{h_1, h_2, h_3\}$ in this chapter, such as in data treatment, texture analysis and stress measurement, are applicable to all goniometer geometries provided that the unit-vector components are generated from the corresponding transformation matrix from diffraction space to the sample space.

2.5.2.4.3. *Transformation from detector space to reciprocal space*

Reciprocal-space mapping is commonly used to analyse the diffraction patterns from highly oriented structures, diffuse scattering from crystal defects, and thin films (Hanna & Windle, 1995; Mudie *et al.*, 2004; Smilgies & Blasini, 2007; Schmidbauer *et al.*, 2008). The equations of the unit-vector calculation given above can also be used to transform the diffraction intensity from the diffraction space to the reciprocal space with respect to the sample coordinates. The direction of the scattering vector is given by the unit vector $\mathbf{h}_s\{h_1, h_2, h_3\}$ and the magnitude of the scattering vector is given by $2\sin\theta/\lambda$, so that the scattering vector corresponding to a pixel is given by

$$\mathbf{H} = \frac{2\sin\theta}{\lambda}\mathbf{h}_s. \tag{2.5.13}$$

The three-dimensional reciprocal-space mapping can be obtained by applying the normalized pixel intensities to the corresponding reciprocal points. With various sample orientations, all pixels on the detector can be mapped into a 3D reciprocal space.

Copyright © 2018 International Union of Crystallography

2.5.3. Instrumentation

2.5.3.1. *X-ray source and optics*

2.5.3.1.1. *Beam path in a diffractometer equipped with a 2D detector*

The Bragg–Brentano (B-B) parafocusing geometry is most commonly used in conventional X-ray diffractometers with a point detector (Cullity, 1978; Jenkins & Snyder, 1996). In the Bragg–Brentano geometry, the sample surface normal is always a bisector between the incident beam and the diffracted beam. A divergent incident beam hits the sample surface with an incident angle θ. The area of the irradiated region depends on the incident angle θ and the size of the divergence slit. The diffracted rays leave the sample at an angle 2θ, pass through the anti-scatter slit and receiving slit, and reach the point detector. Soller slits are used on both the primary side and secondary side to minimize the effects of axial divergence due to the line-focus beam. The primary line-focus beam sliced by the Soller slits can also be considered as an array of point beams parallel to the diffractometer planes. Each of these point beams will produce a diffraction cone from the sample. The overlap of all the diffraction cones will create a smeared diffraction peak. The Soller slits on the receiving side allow only those diffracted beams nearly parallel to the diffractometer plane to pass through, so the smearing effect is minimized. In another words, the so-called 'line-focus geometry' in conventional diffractometry is actually a superposition of many layers of 'spot-focus geometry'.

The beam path in a diffractometer equipped with a 2D detector is different from that in a conventional diffractometer in many respects (He & Preckwinkel, 2002). In a 2D-XRD system the whole or a large portion of the diffraction rings are measured simultaneously, and neither slits nor monochromator can be used between the sample and detector. Therefore, the X-ray source and optics for 2D-XRD systems have different requirements in terms of the beam spectral purity, divergence and beam cross-section profile. Fig. 2.5.9 shows the beam path in a 2D-XRD system with the θ–θ configuration. The geometry for the θ–2θ configuration is equivalent. The X-ray tube, monochromator and collimator assembly are all mounted on the primary side. The incident-beam assembly rotates about the instrument centre and makes an incident angle θ_1 to the sample surface. The first main axis is also called the θ_1 axis. The diffracted beams travel in all directions and some are intercepted by a 2D detector. The detector is mounted on the other main axis, θ_2. The detector position is determined by the sample-to-detector distance D and the detector swing angle α ($= \theta_1 + \theta_2$).

All the components and space between the focal spot of the X-ray tube and sample are collectively referred to as the primary beam path. The primary beam path in a 2D-XRD system is typically sheltered by optical components except between the exit of the collimator and the sample. The X-rays travelling through this open incident-beam path are scattered by the air with two adverse effects. One is the attenuation of the primary beam intensity. The more harmful effect is that the scattered X-rays travel in all directions and some reach the detector, as is shown by the dashed lines with arrows in Fig. 2.5.9. This air scatter introduces a background over the diffraction pattern. Weak diffraction patterns may be buried under the background. Obviously, the air scatter from the incident beam is significantly stronger than that from diffracted X-rays. The intensity of the air scatter from the incident beam is proportional to the length of the open incident-beam path. The effect of air scatter also depends on the wavelength of the X-rays. The longer the wavelength is, the more severe is the air scatter. The secondary beam path is the space between the sample and the 2D detector. The diffracted X-rays are also scattered by air and the diffraction pattern is both attenuated and blurred by the air scattering. In a conventional diffractometer, one can use an anti-scatter slit, diffracted-beam monochromator or detector Soller slits to remove most of the air scatter that is not travelling in the diffracted-beam direction. These measures cannot be used for a 2D-XRD system, which requires an open space between the sample and the 2D detector. Therefore, the open incident-beam path should be kept as small as possible. In order to reduce the air attenuation and air scatter of the incident beam, a helium-purged beam path or a vacuum beam path are sometimes used in a diffractometer. The air scatter from the diffracted X-rays is relatively weak and the effect depends on sample-to-detector distance. It is typically not necessary to take measures to remove air scatter from the diffracted X-rays between the sample and 2D detector if the sample-to-detector distance is 30 cm or less with Cu $K\alpha$ radiation. However, if the sample-to-detector distance is larger than 30 cm or longer-wavelength radiation, such as Co $K\alpha$ or Cr $K\alpha$, is used, it is then necessary to use an He beam path or vacuum beam path to reduce the air scatter.

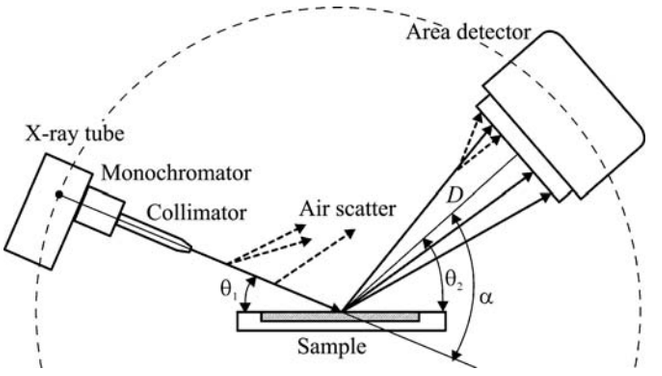

Figure 2.5.9
X-ray beam path in a two-dimensional X-ray diffraction system.

2.5.3.1.2. *Liouville's theorem*

Liouville's theorem can be used to describe the nature of the X-ray source, the X-ray optics and the coupling of the source and optics (Arndt, 1990). Liouville's theorem can be stated in a variety of ways, but for X-ray optics the best known form is

$$S_1\alpha = S_2\beta, \tag{2.5.14}$$

where S_1 is the effective size of the X-ray source and α is the capture angle determined by the effective size of the X-ray optics and the distance between the source and optics. S_2 is the size of the image focus. β is the convergence angle of the X-ray beam from the optics, which is also determined by the effective size of the X-ray optics and the distance between the optics and the image focus. The β angle is also called the crossfire of the X-ray beam. S_2 and β are typically determined by experimental requirements such as beam size and divergence. Therefore, the product $S_1\alpha$ is also determined by experimental conditions. In another expression of Liouville's theorem, the space volume containing the X-ray photons cannot be reduced with time along the trajectories of the system. Therefore, the brilliance of an X-ray source cannot be increased by optics, but may be reduced because of the loss of X-ray photons passing through the optics. In practice, no optics can have 100% reflectivity or transmission.

Considering this, Liouville's theorem given in equation (2.5.14) should be expressed as

$$S_1\alpha \leq S_2\beta. \tag{2.5.15}$$

This states that the product of the divergence and image size can be equal to or greater than the product of the capture angle and source size. If the X-ray source is a point with zero area, the focus image from focusing optics or the cross section of a parallel beam can be any chosen size. For focusing optics, the source size must be considerably smaller than the output beam size in order to achieve a gain in flux. In this case, the flux gain is from the increased capture angle. For parallel optics, the divergence angle β is infinitely small by definition, so it is necessary to use an X-ray source as small as possible to achieve a parallel beam. Focusing optics have an advantage over parallel optics in terms of beam flux. Using an X-ray beam with a divergence much smaller than the mosaicity of the specimen crystal does not improve the resolution, but does sacrifice diffraction intensity. For many X-ray diffraction applications with polycrystalline materials, a large crossfire is acceptable as long as the diffraction peaks concerned can be resolved. The improved peak profile and counting statistics can most often compensate for the peak broadening due to large crossfire.

2.5.3.1.3. *X-ray source*

A variety of X-ray sources, from sealed X-ray tubes and rotating-anode generators to synchrotron radiation, can be used for 2D powder diffraction. The history and principles of X-ray generation can be found in many references (Klug & Alexander, 1974; Cullity, 1978). The X-ray beam intensity depends on the X-ray optics, the focal-spot brightness and the focal-spot profile. The focal-spot brightness is determined by the maximum target loading per unit area of the focal spot, also referred to as the specific loading. A microfocus sealed tube (Bloomer & Arndt, 1999; Wiesmann *et al.*, 2007), which has a very small focal spot size (10–50 µm), can deliver a brilliance as much as one to two orders of magnitude higher than a conventional fine-focus sealed tube. The tube, which is also called a 'microsource', is typically air cooled because the X-ray generator power is less than 50 W. The X-ray optics for a microsource, either a multilayer mirror or a polycapillary, are typically mounted very close to the focal spot so as to maximize the gain on the capture angle. A microsource is highly suitable for 2D-XRD because of its spot focus and high brilliance.

If the X-rays used for diffraction have a wavelength slightly shorter than the *K* absorption edge of the sample material, a significant amount of fluorescent radiation is produced, which spreads over the diffraction pattern as a high background. In a conventional diffractometer with a point detector, the fluorescent background can be mostly removed by either a receiving monochromator mounted in front of the detector or by using a point detector with sufficient energy resolution. However, it is impossible to add a monochromator in front of a 2D detector and most area detectors have insufficient energy resolution. In order to avoid intense fluorescence, the wavelength of the X-ray-tube $K\alpha$ line should either be longer than the *K* absorption edge of the sample or far away from the *K* absorption edge. For example, Cu $K\alpha$ should not be used for samples containing significant amounts of the elements iron or cobalt. Since the $K\alpha$ line of an element cannot excite fluorescence of the same element, it is safe to use an anode of the same metallic element as the sample if the X-ray tube is available, for instance Co $K\alpha$ for Co samples. In general, intense fluorescence is produced when the atomic number of the anode material is 2, 3, or 4 larger than that of an element in the sample. When the sample contains Co, Fe or Mn (or Ni or Cu), the use of Cu $K\alpha$ radiation should be avoided; similarly, one should avoid using Co $K\alpha$ radiation if the sample contains Mn, Cr or V, and avoid using Cr $K\alpha$ radiation if the sample contains Ti, Sc or Ca. The effect is reduced when the atomic-number difference increases.

2.5.3.1.4. *X-ray optics*

The function of the X-ray optics is to condition the primary X-ray beam into the required wavelength, beam focus size, beam profile and divergence. Since the secondary beam path in a 2D-XRD system is an open space, almost all X-ray optics components are on the primary side. The X-ray optics components commonly used for 2D-XRD systems include a β-filter, a crystal monochromator, a pinhole collimator, cross-coupled multilayer mirrors, a Montel mirror, a polycapillary and a monocapillary. Detailed descriptions of these optic devices can be found in Chapter 2.1. In principle, the cross-sectional shape of the X-ray beam used in a 2D diffraction system should be small and round. In data-analysis algorithms, the beam size is typically considered to be a point. In practice, the beam cross section can be either round, square or another shape with a limited size. Such an X-ray beam is typically collimated or conditioned by the X-ray optics in two perpendicular directions, so that the X-ray optics used for the point beam are often called 'two-dimensional X-ray optics'.

A pinhole collimator is normally used to control the beam size and divergence in addition to other optic devices. The choice of beam size is often a trade-off between intensity and the ability to illuminate small regions or resolve closely spaced sample features. Smaller beam sizes, such as 50 µm and 100 µm, are preferred for microdiffraction and large beam sizes, such as 0.5 mm or 1 mm, are typically used for quantitative analysis, or texture or crystallinity measurements. In the case of quantitative analysis and texture measurements, using too small a collimator can actually be a detriment, causing poor grain-sampling statistics. The smaller the collimator, the longer the data-collection time. The beam divergence is typically determined by both the collimator and the coupling optic device. Lower divergence is typically associated with a long beam path. At the same time, the beam flux is inversely proportional to the square of the distance between the source and the sample. There are two main factors determining the length of the primary beam path: the first is the required distance for collimating the beam into the required divergence, the second is the space required for the primary X-ray optics, the sample stage and the detector. On the condition that the above two factors are satisfied, the primary X-ray beam path should be kept as short as possible.

2.5.3.2. *2D detector*

Two-dimensional (2D) detectors, also referred to as area detectors, are the core of 2D-XRD. The advances in area-detector technologies have inspired applications both in X-ray imaging and X-ray diffraction. A 2D detector contains a two-dimensional array of detection elements which typically have identical shape, size and characteristics. A 2D detector can simultaneously measure both dimensions of the two-dimensional distribution of the diffracted X-rays. Therefore, a 2D detector may also be referred to as an X-ray camera or imager. There are many technologies for area detectors (Arndt, 1986; Krause & Phillips, 1992; Eatough *et al.*, 1997; Giomatartis, 1998; Westbrook,

1999; Durst *et al.*, 2002; Blanton, 2003; Khazins *et al.*, 2004). X-ray photographic plates and films were the first generation of two-dimensional X-ray detectors. Now, multiwire proportional counters (MWPCs), image plates (IPs), charge-coupled devices (CCDs) and microgap detectors are the most commonly used large area detectors. Recent developments in area detectors include X-ray pixel array detectors (PADs), silicon drift diodes (SDDs) and complementary metal-oxide semiconductor (CMOS) detectors (Ercan *et al.*, 2006; Lutz, 2006; Yagi & Inoue, 2007; He *et al.*, 2011). Each detector type has its advantages over the other types. In order to make the right choice of area detector for a 2D-XRD system and applications, it is necessary to characterize area detectors with consistent and comparable parameters. Chapter 2.1 has more comprehensive coverage on X-ray detectors, including area detectors. This section will cover the characteristics specifically relevant to area detectors.

2.5.3.2.1. *Active area and pixel size*

A 2D detector has a limited detection surface and the detection surface can be spherical, cylindrical or flat. The detection-surface shape is also determined by the detector technology. For example, a CCD detector is made from a large semiconductor wafer, so that only a flat CCD is available, while an image plate is flexible so that it is easily bent to a cylindrical shape. The area of the detection surface, also referred to as the active area, is one of the most important parameters of a 2D detector. The larger the active area of a detector, the larger the solid angle that can be covered at the same sample-to-detector distance. This is especially important when the instrumentation or sample size forbid a short sample-to-detector distance. The active area is also limited by the detector technology. For instance, the active area of a CCD detector is limited by the semiconductor wafer size and fabrication facility. A large active area can be achieved by using a large demagnification optical lens or fibre-optical lens. Stacking several CCD chips side-by-side to build a so-called mosaic CCD detector is another way to achieve a large active area.

In addition to the active area, the overall weight and dimensions are also very important factors in the performance of a 2D detector. The weight of the detector has to be supported by the goniometer, so a heavy detector means high demands on the size and power of the goniometer. In a vertical configuration, a heavy detector also requires a heavy counterweight to balance the driving gear. The overall dimensions of a 2D detector include the height, width and depth. These dimensions determine the manoeuvrability of the detector within a diffractometer, especially when a diffractometer is loaded with many accessories, such as a video microscope and sample-loading mechanism. Another important parameter of a 2D detector that tends to be ignored by most users is the blank margin surrounding the active area of the detector. Fig. 2.5.10 shows the relationship between the maximum measurable 2θ angle and the detector blank margin. For high 2θ angle measurements, the detector swing angle is set so that the incident X-ray optics are set as closely as possible to the detector. The unmeasurable blank angle is the sum of the detector margin m and the dimension from the incident X-ray beam to the outer surface of the optic device h. The maximum measurable angle is given by

$$2\theta_{\max} = \pi - \frac{m+h}{D}. \qquad (2.5.16)$$

It can be seen that either reducing the detector blank margin or optics blank margin can increase the maximum measurable angle.

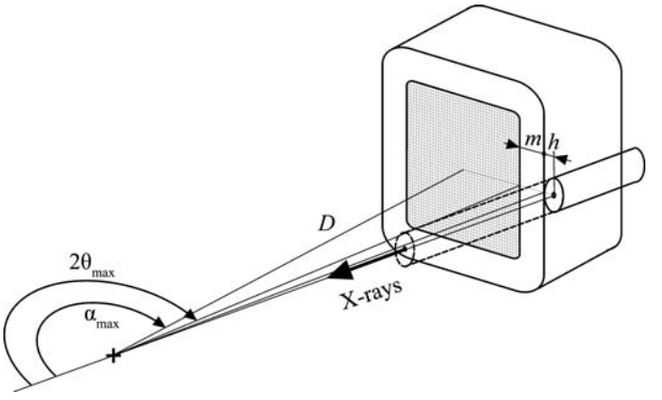

Figure 2.5.10
Detector dimensions and maximum measurable 2θ.

The solid angle covered by a pixel in a flat detector is dependent on the sample-to-detector distance and the location of the pixel in the detector. Fig. 2.5.11 illustrates the relationship between the solid angle covered by a pixel and its location in a flat area detector. The symbol S may represent a sample or a calibration source at the instrument centre. The distance between the sample S and the detector is D. The distance between any arbitrary pixel $P(x, y)$ and the detector centre pixel $P(0, 0)$ is r. The pixel size is Δx and Δy (assuming $\Delta x = \Delta y$). The distance between the sample S and the pixel is R. The angular ranges covered by this pixel are $\Delta\alpha$ and $\Delta\beta$ in the x and y directions, respectively. The solid angle covered by this pixel, $\Delta\Omega$, is then given as

$$\Delta\Omega = \Delta\alpha\Delta\beta = \frac{D}{R^3}\Delta y\Delta x = \frac{D}{R^3}\Delta A, \qquad (2.5.17)$$

where $\Delta A = \Delta x\Delta y$ is the area of the pixel and R is given by

$$R = (D^2 + x^2 + y^2)^{1/2} = (D^2 + r^2)^{1/2}. \qquad (2.5.18)$$

When a homogeneous calibration source is used, the flux to a pixel at $P(x, y)$ is given as

$$F(x, y) = \Delta\Omega B = \frac{\Delta ADB}{R^3} = \frac{\Delta ADB}{(D^2 + x^2 + y^2)^{3/2}}, \qquad (2.5.19)$$

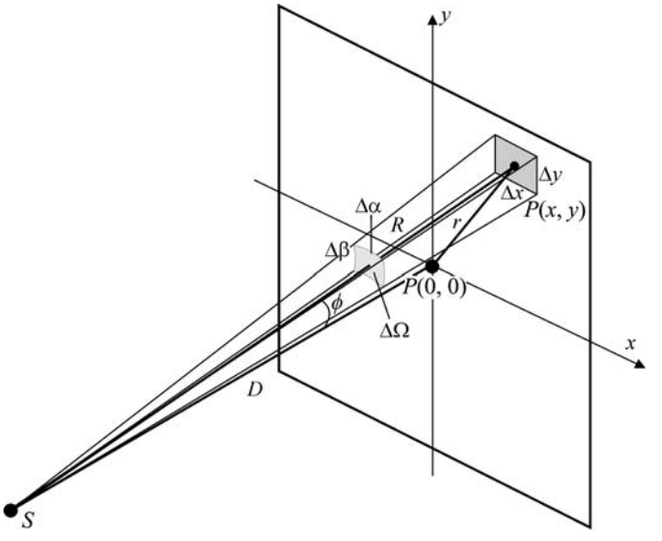

Figure 2.5.11
Solid angle covered by each pixel and its location on the detector.

where $F(x, y)$ is the flux (in photons s^{-1}) intercepted by the pixel and B is the brightness of the source (in photons s^{-1} $mrad^{-2}$) or scattering from the sample. The ratio of the flux in pixel $P(x, y)$ to that in the centre pixel $P(0, 0)$ is then given as

$$\frac{F(x, y)}{F(0, 0)} = \frac{D^3}{R^3} = \frac{D^3}{(D^2 + x^2 + y^2)^{3/2}} = \cos^3\phi, \qquad (2.5.20)$$

where ϕ is the angle between the X-rays to the pixel $P(x, y)$ and the line from S to the detector in perpendicular direction. It can be seen that the greater the sample-to-detector distance, the smaller the difference between the centre pixel and the edge pixel in terms of the flux from the homogeneous source. This is the main reason why a data frame collected at a short sample-to-detector distance has a higher contrast between the edge and centre than one collected at a long sample-to-detector distance.

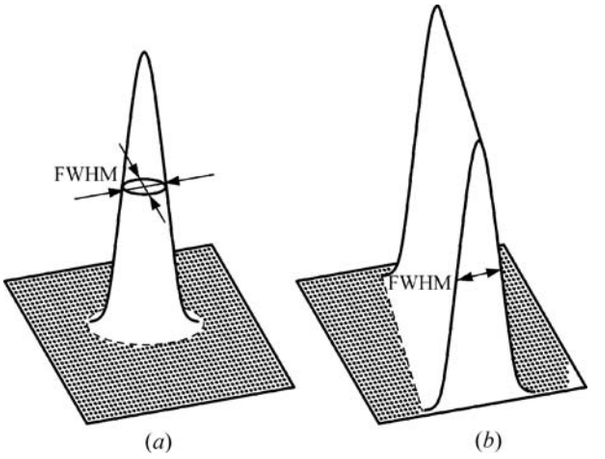

Figure 2.5.12
(*a*) Point-spread function (PSF) from a parallel point beam; (*b*) line-spread function (LSF) from a sharp line beam.

2.5.3.2.2. *Spatial resolution of area detectors*

In a 2D diffraction frame, each pixel contains the X-ray intensity collected by the detector corresponding to the pixel element. The pixel size of a 2D detector can be determined by or related to the actual feature sizes of the detector structure, or artificially determined by the readout electronics or data-acquisition software. Many detector techniques allow multiple settings for variable pixel size, for instance a frame of 2048 × 2048 pixels or 512 × 512 pixels. Then the pixel size in 512 mode is 16 (4 × 4) times that of a pixel in 2048 mode. The pixel size of a 2D detector determines the space between two adjacent pixels and also the minimum angular steps in the diffraction data, therefore the pixel size is also referred to as pixel resolution.

The pixel size does not necessarily represent the true spatial resolution or the angular resolution of the detector. The resolving power of a 2D detector is also limited by its point-spread function (PSF) (Bourgeois *et al.*, 1994). The PSF is the two-dimensional response of a 2D detector to a parallel point beam smaller than one pixel. When the sharp parallel point beam strikes the detector, not only does the pixel directly hit by the beam record counts, but the surrounding pixels may also record some counts. The phenomenon is observed as if the point beam has spread over a certain region adjacent to the pixel. In other words, the PSF gives a mapping of the probability density that an X-ray photon is recorded by a pixel in the vicinity of the point where the X-ray beam hits the detector. Therefore, the PSF is also referred to as the spatial redistribution function. Fig. 2.5.12(*a*) shows the PSF produced from a parallel point beam. A plane at half the maximum intensity defines a cross-sectional region within the PSF. The FWHM can be measured at any direction crossing the centroid of the cross section. Generally, the PSF is isotropic, so the FWHMs measured in any direction should be the same.

Measuring the PSF directly by using a small parallel point beam is difficult because the small PSF spot covers a few pixels and it is hard to establish the distribution profile. Instead, the line-spread function (LSF) can be measured with a sharp line beam from a narrow slit (Ponchut, 2006). Fig. 2.5.12(*b*) is the intensity profile of the image from a sharp line beam. The LSF can be obtained by integrating the image from the line beam along the direction of the line. The FWHM of the integrated profile can be used to describe the LSF. Theoretically, LSF and PSF profiles are not equivalent, but in practice they are not distinguished and may be referenced by the detector specification interchangeably. For accurate LSF measurement, the line beam is intentionally positioned with a tilt angle from the orthogonal direction of the pixel array so that the LSF can have smaller steps in the integrated profile (Fujita *et al.*, 1992).

The RMS (root-mean-square) of the distribution of counts is another parameter often used to describe the PSF. The normal distribution, also called the Gaussian distribution, is the most common shape of a PSF. The RMS of a Gaussian distribution is its standard deviation, σ. Therefore, the FWHM and RMS have the following relation, assuming that the PSF has a Gaussian distribution:

$$\text{FWHM} = 2[-2\ln(1/2)]^{1/2}\text{RMS} = 2.3548 \times \text{RMS}. \qquad (2.5.21)$$

The values of the FWHM and RMS are significantly different, so it is important to be precise about which parameter is used when the value is given for a PSF.

For most area detectors, the pixel size is smaller than the FWHM of the PSF. The pixel size should be small enough that at least a 50% drop in counts from the centre of the PSF can be observed by the pixel adjacent to the centre pixel. In practice, an FWHM of 3 to 6 times the pixel size is a reasonable choice if use of a smaller pixel does not have other detrimental effects. A further reduction in pixel size does not necessarily improve the resolution. Some 2D detectors, such as pixel-array detectors, can achieve a single-pixel PSF. In this case, the spatial resolution is determined by the pixel size.

2.5.3.2.3. *Detective quantum efficiency and energy range*

The detective quantum efficiency (DQE), also referred to as the detector quantum efficiency or quantum counting efficiency, is measured by the percentage of incident photons that are converted by the detector into electrons that constitute a measurable signal. For an ideal detector, in which every X-ray photon is converted to a detectable signal without additional noise added, the DQE is 100%. The DQE of a real detector is less than 100% because not every incident X-ray photon is detected, and because there is always some detector noise. The DQE is a parameter defined as the square of the ratio of the output and input signal-to-noise ratios (SNRs) (Stanton *et al.*, 1992):

$$\text{DQE} = \left(\frac{(S/N)_{\text{out}}}{(S/N)_{\text{in}}}\right)^2. \qquad (2.5.22)$$

The DQE of a detector is affected by many variables, for example the X-ray photon energy and the counting rate. The dependence of the DQE on the X-ray photon energy defines the

energy range of a detector. The DQE drops significantly if a detector is used out of its energy range. For instance, the energy range of MWPC and microgap detectors is about 3 to 15 keV. The DQE with Cu $K\alpha$ radiation (8.06 keV) is about 80%, but drops gradually when approaching the lower or higher energy limits. The energy range of imaging plates is much wider (4–48 keV). The energy range of a CCD, depending on the phosphor, covers from 5 keV up to the hard X-ray region.

2.5.3.2.4. *Detection limit and dynamic range*

The detection limit is the lowest number of counts that can be distinguished from the absence of true counts within a specified confidence level. The detection limit is estimated from the mean of the noise, the standard deviation of the noise and some confidence factor. In order to have the incoming X-ray photons counted with a reasonable statistical certainty, the counts produced by the X-ray photons should be above the detector background-noise counts.

The dynamic range is defined as the range extending from the detection limit to the maximum count measured in the same length of counting time. The linear dynamic range is the dynamic range within which the maximum counts are collected within the specified linearity. For X-ray detectors, the dynamic range most often refers to linear dynamic range, since only a diffraction pattern collected within the linear dynamic range can be correctly interpreted and analysed. When the detection limit in count rate approaches the noise rate at extended counting time, the dynamic range can be approximated by the ratio of the maximum count rate to the noise rate.

Dynamic range is very often confused with the maximum count rate, but must be distinguished. With a low noise rate, a detector can achieve a dynamic range much higher than its count rate. For example, if a detector has a maximum linear count rate of 10^5 s^{-1} with a noise rate of 10^{-3} s^{-1}, the dynamic range can approach 10^8 for an extended measurement time. The dynamic range for a 2D detector has the same definition as for a point detector, except that with a 2D detector the whole dynamic range extending from the detection limit to the maximum count can be observed from different pixels simultaneously. In order to record the entire two-dimensional diffraction pattern, it is necessary for the dynamic range of the detector to be at least the dynamic range of the diffraction pattern, which is typically in the range 10^2 to 10^6 for most applications. If the range of reflection intensities exceeds the dynamic range of the detector, then the detector will either saturate or have low-intensity patterns truncated. Therefore, it is desirable that the detector has as large a dynamic range as possible.

2.5.3.2.5. *Types of 2D detectors*

2D detectors can be classified into two broad categories: photon-counting detectors and integrating detectors (Lewis, 1994). Photon-counting area detectors can detect a single X-ray photon entering the active area. In a photon-counting detector, each X-ray photon is absorbed and converted to an electrical pulse. The number of pulses counted per unit time is proportional to the incident X-ray flux. Photon-counting detectors typically have high counting efficiency, approaching 100% at low count rate. The most commonly used photon-counting 2D detectors include MWPCs, Si-pixel arrays and microgap detectors. Integrating area detectors, also referred to as analogue X-ray imagers, record the X-ray intensity by measuring the analogue electrical signals converted from the incoming X-ray flux. The signal size of each pixel is proportional to the fluence of incident X-rays. The most commonly used integrating 2D detectors include image plates (IPs) and charge-coupled devices (CCDs).

The selection of an appropriate 2D detector depends on the X-ray diffraction application, the sample condition and the X-ray beam intensity. In addition to geometry features, such as the active area and pixel format, the most important performance characteristics of a detector are its sensitivity, dynamic range, spatial resolution and background noise. The detector type, either photon-counting or integrating, also leads to important differences in performance. Photon-counting 2D detectors typically have high counting efficiency at low count rate, while integrating 2D detectors are not so efficient at low count rate because of the relatively high noise background. An MWPC has a high DQE of about 0.8 when exposed to incoming local fluence from single photons up to about 10^3 photons s^{-1} mm^{-2}. The diffracted X-ray intensities from a polycrystalline or powder sample with a typical laboratory X-ray source fall into this fluence range. This is especially true with microdiffraction, where high sensitivity and low noise are crucial to reveal the weak diffraction pattern. Owing to the counting losses at a high count rate, the DQE of an MWPC decreases with increasing count rate and quickly saturates above 10^3 photons s^{-1} mm^{-2}. Therefore, an MWPC is not suitable for collecting strong diffraction patterns or for use with high intensity sources, such as synchrotron X-ray sources. An IP can be used in a large fluence range from 10 photons s^{-1} mm^{-2} and up with a DQE of 0.2 or lower. An IP is suitable for strong diffraction from single crystals with high-intensity X-ray sources, such as a rotating-anode generator or synchrotron X-ray source. With weak diffraction signals, the image plate cannot resolve the diffraction data near the noise floor. A CCD detector can also be used over a large X-ray fluence range from 10 photons s^{-1} mm^{-2} to very high fluence with a much higher DQE of 0.7 or higher. It is suitable for collecting diffraction of medium to strong intensity from single-crystal or polycrystalline samples. Owing to the relatively high sensitivity and high local count rate, CCDs can be used in systems with either sealed-tube X-ray sources, rotating-anode generators or synchrotron X-ray sources. With a low DQE at low fluence and the presence of dark-current noise, a CCD is not a good choice for applications with weak diffraction signals. A microgap detector has the best combination of high DQE, low noise and high count rate. It has a DQE of about 0.8 at an X-ray fluence from single photons up to about 10^5 photons s^{-1} mm^2. It is suitable for microdiffraction when high sensitivity and low noise are crucial to reveal weak diffraction patterns. It can also handle high X-ray fluence from strong diffraction patterns or be used with high-intensity sources, such as rotating-anode generators or synchrotron X-ray sources.

2.5.3.3. *Data corrections and integration*

2D diffraction patterns contain abundant information. In order to interpret and analyse 2D patterns accurately it is necessary to apply some data-treatment processes (Sulyanov *et al.*, 1994; Scheidegger *et al.*, 2000; Cervellino *et al.*, 2006; Boesecke, 2007; Rowe, 2009). Most data-treatment processes can be categorized as having one of the following four purposes: to eliminate or reduce errors caused by detector defects; to remove undesirable effects of instrument and sample geometry; to transfer a 2D frame into a format such that the data can be presented or further analysed by conventional means and software; and cosmetic treatment, such as smoothing a frame for reports and publications.

2.5.3.3.1. *Nonuniform response correction*

A 2D detector can be considered as an array of point detectors. Each pixel may have its own response, and thus a 2D detector may exhibit some nonuniformity in intensity measurement when exposed to an isotropic source. The nonuniform response can be caused by manufacturing defects, inadequate design or limitations of the detector technology. For instance, a nonuniform phosphor screen or coupling fibre optic for a CCD detector may cause nonuniformity in quantum efficiency (Tate *et al.*, 1995). A gas-filled detector may have a different intensity response between the detector edge and centre due to the variation in the electric field from the centre to the edge. A thorough correction to the nonuniformity of the intensity response can be performed if the detector counting curves of all pixels are given. In practice, this is extremely difficult or impossible, because the behaviour of a pixel may be affected by the condition of the adjacent pixels and the whole detector. The practical way to correct the nonuniformity of the intensity response is to collect an X-ray image from an isotropic point source at the instrument centre and use the image data frame to generate a correction table for the future diffraction frames. The frame collected with the isotropic source is commonly referred to as a 'flood-field' frame or a flat-field image, and the correction is also called a flood-field correction or flat-field correction (Stanton *et al.*, 1992). Another type of correction for a nonuniform response is background correction. Background correction is done by subtracting a background frame from the data frame. The background frame is collected without X-ray exposure. Integrating detectors, such as image plates or CCDs, have a strong background which must be considered in nonuniform response correction. Photon-counting detectors, such as MWPC and microgap detectors, have negligible background, so background correction is not necessary.

The X-ray source for calibration for flood-field correction should be a uniform, spherically radiating point source. Identical brightness should be observed at any pixel on the detector. The radiation strength of the source should match the intensity of the diffraction data to be collected. The photon energy of the source should be the same as or close to the X-ray beam used for diffraction-data collection so that the detector behaves the same way during calibration and data collection.

There are many choices of calibration sources, including X-ray tubes, radioactive sources, diffuse scattering or X-ray fluorescence. The radioactive source Fe-55 (^{55}Fe) is the most commonly used calibration source for a diffraction system because of its major photon energy level of 5.9 keV. X-ray fluorescence is an alternative to a radioactive source. Fluorescence emission is generated by placing a fluorescent material into the X-ray beam. Fluorescence radiation is an isotopic point source if the irradiated area is a small point-like area. For example, Cu $K\alpha$ can produce intense fluorescence from materials containing significant amounts of iron or cobalt and Mo $K\alpha$ can produce intense fluorescence from materials containing yttrium. In order to avoid a high localized intensity contribution from X-ray diffraction, the fluorescent material should be amorphous, such as a glassy iron foil. An alternative to a glassy alloy foil is amorphous lithium borate glass doped with the selected fluorescent element up to a 10% concentration (Moy *et al.*, 1996).

There are many algorithms available for flood-field correction depending on the nature of the 2D detector. The correction is based on the flood-field frame collected from the calibration source. The simplest flood-field correction is to normalize the counts of all pixels to the same level assuming that all pixels have the same response curve. The corrected frame from an isotropic source is not flat, but maintains the $\cos^3 \phi$ falloff effect, which will be considered in the frame integration. For gas-filled detectors, such as MWPC and microgap detectors, the pixel intensity response is not independent, but is affected by X-ray exposure to surrounding pixels and the whole detector. Flood-field correction is carried out by applying a normalization factor to each pixel in which a 'rubber-sheet' kind of stretching and shrinking in regions along the x and y detector axes slightly alters the size of each pixel (He, 2009). The total number of counts remains the same after the correction but is redistributed throughout the pixels so that the image from an isotropic source is uniformly distributed across the detector. The flood-field calibration must be done with the same sample-to-detector distance as for the diffraction-data collection.

2.5.3.3.2. *Spatial correction*

In an ideal flat 2D detector, not only does each pixel have the same intensity response, but also an accurate position. The pixels are aligned in the x and y directions with equal spacing. In most cases we assume that the detective area is completely filled by pixels, so the distance between two neighbouring pixels is equivalent to the pixel size. The deviation from this perfect pixel array is called spatial distortion. The extent of spatial distortion is dependent on the nature and limitation of the detector technology. A CCD detector with 1:1 demagnification may have a negligible spatial distortion, but the barrel distortion in the coupling fibre-optic taper can introduce substantial spatial distortion. An image-plate system may have spatial distortion caused by imperfections in the scanning system (Campbell *et al.*, 1995). MWPC detectors typically exhibit more severe spatial distortion due to the window curvature and imperfections in the wire anode (Derewenda & Helliwell, 1989).

The spatial distortion is measured from X-ray images collected with a uniformly radiating point source positioned at the instrument centre and a fiducial plate fastened to the front surface of the detector. The source for spatial correction should have a very accurate position, point-like shape and small size. The fiducial plate is a metal plate with accurately distributed pinholes in the x and y directions. The X-ray image collected with this setup contains sharp peaks corresponding to the pinhole pattern of the fiducial plate. Since accurate positions of the peaks are given by the fiducial plate, the spatially corrected image is a projection of the collected image to this plane. Therefore, the detector plane is defined as the contacting plane between the fiducial plate and detector front face.

Spatial correction restores the spatially distorted diffraction frame into a frame with correct pixel positions. Many algorithms have been suggested for spatial correction (Sulyanov *et al.*, 1994; Tate *et al.*, 1995; Stanton *et al.*, 1992; Campbell *et al.*, 1995). In the spatially corrected frame each pixel is generated by computing the pixel count from the corresponding pixels based on a spatial-correction look-up table. In a typical spatial-correction process, an image containing the spots from the calibration source passing through the fiducial plate is collected. The distortion of the image is revealed by the fiducial spots. Based on the known positions of the corresponding pinholes in the fiducial plate, the distortion of each fiducial spot can be determined. The spatial correction for all pixels can be calculated and stored as a look-up table. Assuming that the detector behaves the same way in the real diffraction-data collection, the look-up table generated from the fiducial image can then be applied to the real diffraction frames.

The spatial calibration must be done at the same sample-to-detector distance as the diffraction-data collection.

2.5.3.3.3. *Frame integration*

2D frame integration is a data-reduction process which converts a two-dimensional frame into a one-dimensional intensity profile. Two forms of integration are generally of interest in the analysis of a 2D diffraction frame from polycrystalline materials: γ integration and 2θ integration. γ integration sums the counts in 2θ steps ($\Delta 2\theta$) along constant 2θ conic lines and between two constant γ values. γ integration produces a data set with intensity as a function of 2θ. 2θ integration sums the counts in γ steps ($\Delta\gamma$) along constant γ lines and between two constant 2θ conic lines. 2θ integration produces a data set with intensity as a function of γ. γ integration may also be carried out with the integration range in the vertical direction as a constant number of pixels. This type of γ integration may also be referred to as slice integration. A diffraction profile analogous to the conventional diffraction result can be obtained by either γ integration or slice integration over a selected 2θ range. Phase ID can then be done with conventional search/match methods. 2θ integration is of interest for evaluating the intensity variation along γ angles, such as for texture analysis, and is discussed in more depth in Chapter 5.3.

The γ integration can be expressed as

$$I(2\theta) = \int_{\gamma_1}^{\gamma_2} J(2\theta, \gamma)\, \mathrm{d}\gamma, \quad 2\theta_1 \leq 2\theta \leq 2\theta_2, \tag{2.5.23}$$

where $J(2\theta, \gamma)$ represents the two-dimensional intensity distribution in the 2D frame and $I(2\theta)$ is the integration result as a function of intensity *versus* 2θ. γ_1 and γ_2 are the lower limit and upper limit of integration, respectively, which are constants for γ integration. Fig. 2.5.13 shows a 2D diffraction frame collected from corundum (α-Al_2O_3) powder. The 2θ range is from 20 to 60° and the 2θ integration step size is 0.05°. The γ-integration range is from 60 to 120°. In order to reduce or eliminate the dependence of the integrated intensity on the integration interval, the integrated value at each 2θ step is normalized by the number of pixels, the arc length or the solid angle. γ integration with normalization by the solid angle can be expressed as

$$I(2\theta) = \frac{\int_{\gamma_1}^{\gamma_2} J(2\theta, \gamma)(\Delta 2\theta)\, \mathrm{d}\gamma}{\int_{\gamma_1}^{\gamma_2} (\Delta 2\theta)\, \mathrm{d}\gamma}, \quad 2\theta_1 \leq 2\theta \leq 2\theta_2. \tag{2.5.24}$$

Since the $\Delta 2\theta$ step is a constant, the above equation becomes

$$I(2\theta) = \frac{\int_{\gamma_1}^{\gamma_2} J(2\theta, \gamma)\, \mathrm{d}\gamma}{\gamma_2 - \gamma_1}, \quad 2\theta_1 \leq 2\theta \leq 2\theta_2. \tag{2.5.25}$$

There are many integration software packages and algorithms available for reducing 2D frames into 1D diffraction patterns for polycrystalline materials (Cervellino *et al.*, 2006; Rodriguez-Navarro, 2006; Boesecke, 2007). With the availability of tremendous computer power today, a relatively new method is the bin method, which treats pixels as having a continuous distribution in the detector. It demands more computer power than older methods, but delivers much more accurate and smoother results even with $\Delta 2\theta$ integration steps significantly smaller than the pixel size. Depending on the relative size of $\Delta 2\theta$ to the pixel size, each contributing pixel is divided into several 2θ 'bins'. The intensity counts of all pixels within the $\Delta 2\theta$ step are summarized. All the normalization methods in the above integration, either by pixel, arc or solid angle, result in an intensity level of one pixel or unit solid angle. Since a pixel is much smaller than the active area of a typical point detector, the normalized integration tends to result in a diffraction pattern with fictitiously low intensity counts, even though the true counts in the corresponding $\Delta 2\theta$ range are significantly higher. In order to avoid this misleading outcome, it is reasonable to introduce a scaling factor. However, there is no accurate formula for making the integrated profile from a 2D frame comparable to that from a conventional point-detector scan. The best practice is to be aware of the differences and to try not to make direct comparisons purely based on misleading intensity levels. Generally speaking, for the same exposure time, the total counting statistics from a 2D detector are significantly better than from a 0D or 1D detector.

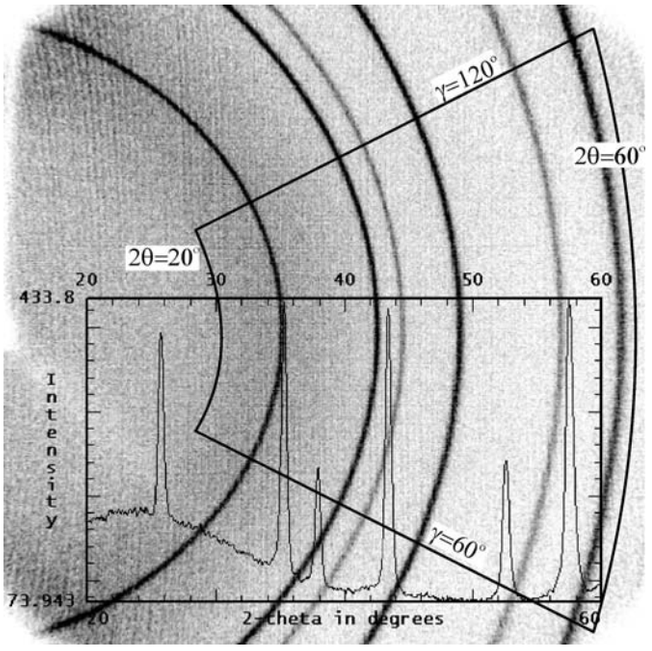

Figure 2.5.13
A 2D frame showing γ integration.

2.5.3.3.4. *Lorentz, polarization and absorption corrections*

Lorentz and polarization corrections may be applied to the diffraction frame to remove their effect on the relative intensities of Bragg peaks and background. The 2θ angular dependence of the relative intensity is commonly given as a Lorentz–polarization factor, which is a combination of Lorentz and polarization factors. In 2D diffraction, the polarization factor is a function of both 2θ and γ, therefore it should be treated in the 2D frames, while the Lorentz factor is a function of 2θ only. The Lorentz correction can be done either on the 2D frames or on the integrated profile. In order to obtain relative intensities equivalent to a conventional diffractometer with a point detector, reverse Lorentz and polarization corrections may be applied to the frame or integrated profile.

The Lorentz factor is the same as for a conventional diffractometer. For a sample with a completely random orientation distribution of crystallites, the Lorentz factor is given as

$$L = \frac{\cos\theta}{\sin^2 2\theta} = \frac{1}{4\sin^2\theta\cos\theta}. \tag{2.5.26}$$

The Lorentz factor may be given by a different equation for a different diffraction geometry (Klug & Alexander, 1974). The forward and reverse Lorentz corrections are exactly reciprocal

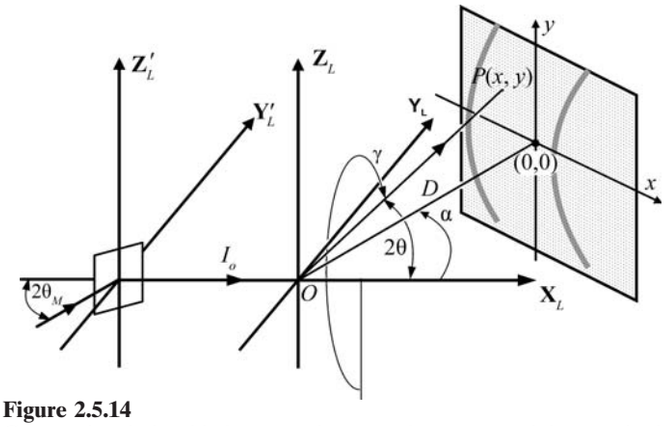

Figure 2.5.14
Geometric relationship between the monochromator and detector in the laboratory coordinates.

and effectively cancel each other. Therefore, it is not necessary to perform the Lorentz correction to the frame before integration if relative intensities equivalent to a conventional Bragg–Brentano diffractometer are expected. The Lorentz correction can be done on the integrated diffraction profiles in the same way as on the diffraction profiles collected with conventional diffractometers.

When a non-polarized X-ray beam is scattered by matter, the scattered X-rays are polarized. The intensity of the diffracted beam is affected by the polarization; this effect is expressed by the polarization factor. In two-dimensional X-ray diffraction the diffraction vectors of the monochromator diffraction and sample crystal diffraction are not necessarily in the same plane or perpendicular planes. Therefore, the overall polarization factor is a function of both 2θ and γ. Fig. 2.5.14 illustrates the geometric relationship between the monochromator and detector in the laboratory coordinates, X_L, Y_L, Z_L. The monochromator is located at the coordinates X_L, Y'_L, Z'_L, which is a translation of the laboratory coordinates along the X_L axis in the negative direction. The monochromator crystal is rotated about the Z'_L axis and $2\theta_M$ is the Bragg angle of the monochromator crystal. The diffracted beam from the monochromator propagates along the X_L direction. This is the incident beam to the sample located at the instrument centre O. The 2D detector location is given by the sample-to-detector distance D and swing angle α. The pixel $P(x, y)$ represents an arbitrary pixel on the detector. 2θ and γ are the corresponding diffraction-space parameters for the pixel. Since a monochromator or other beam-conditioning optics can only be used on the incident beam, the polarization factor for 2D-XRD can then be given as a function of both θ and γ:

$$P(\theta, \gamma) = \frac{(1 + \cos^2 2\theta_M \cos^2 2\theta)\sin^2\gamma + (\cos^2 2\theta_M + \cos^2 2\theta)\cos^2\gamma}{1 + \cos^2 2\theta_M}. \quad (2.5.27)$$

If the crystal monochromator rotates about the Y'_L axis, *i.e.* the incident plane is perpendicular to the diffractometer plane, the polarization factor for two-dimensional X-ray diffraction can be given as

$$P(\theta, \gamma) = \frac{(1 + \cos^2 2\theta_M \cos^2 2\theta)\cos^2\gamma + (\cos^2 2\theta_M + \cos^2 2\theta)\sin^2\gamma}{1 + \cos^2 2\theta_M}. \quad (2.5.28)$$

In the above equations, the term $\cos^2 2\theta_M$ can be replaced by $\left|\cos^n 2\theta_M\right|$ for different monochromator crystals. For a mosaic crystal, such as a graphite crystal, $n = 2$. For most real monochromator crystals, the exponent n takes a value between 1 and 2. For near perfect monochromator crystals, n approaches 1 (Kerr & Ashmore, 1974). All the above equations for polarization factors may apply to multilayer optics. However, since multilayer optics have very low Bragg angles, $\left|\cos^n 2\theta_M\right|$ approximates to unity. The γ dependence of the polarization factor diminishes in this case. The polarization factor approaches

$$P(\theta, \gamma) \simeq \frac{1 + \cos^2 2\theta}{2}. \quad (2.5.29)$$

2.5.3.3.5. *Air scatter*

X-rays are scattered by air molecules in the beam path between the X-ray source and detector. Air scatter results in two effects: one is the attenuation of the X-ray intensity, the other is added background in the diffraction pattern. Air scatter within the enclosed primary beam path – for instance, in the mirror, monochromator housing or collimator – results in attenuation of only the incident beam. The enclosed beam path can be purged by helium gas or kept in vacuum to reduce the attenuation so that no correction is necessary for this part of the air scatter. The open beam between the tip of the collimator and the sample generates an air-scatter background pattern, which is the major part of the air scatter. In the secondary beam path, the air scatter from the diffracted beam may generate background too, but the main effect of the air scatter is inhomogeneous attenuation of the diffraction pattern due to the different beam path lengths between the centre and the edge of the detector.

The background generated by air scattering from the open incident-beam path has a strong 2θ dependence. The specific scattering curve depends on the length of the open primary beam path, the beam size and the wavelength of the incident beam. There are two approaches to correct air scatter. One is to collect an air-scatter background frame under the same conditions as the diffraction frame except without a sample. The background frame is then subtracted from the diffraction frame. Another approach is to remove the background from the integrated profile, since the background is 2θ dependent.

The attenuation of the diffracted beam by air absorption depends on the distance between the sample and pixel. For a flat detector, air absorption can be corrected by

$$p_c(x, y) = p_o(x, y)\exp\left[\mu_{\text{air}}(D^2 + x^2 + y^2)^{1/2}\right], \quad (2.5.30)$$

where $p_o(x, y)$ is the original pixel intensity of the pixel $P(x, y)$ and $p_c(x, y)$ is the corrected intensity. The detector centre is given by $(0, 0)$. μ_{air} is the linear absorption coefficient of air. The value of μ_{air} is determined by the radiation wavelength. By approximation, for air with 80% N_2 and 20% O_2 at sea level and at 293 K, $\mu_{\text{air}} = 0.01\ \text{cm}^{-1}$ for Cu $K\alpha$ radiation. Air scatter and absorption increases with increasing wavelength. For example, $\mu_{\text{air}} = 0.015\ \text{cm}^{-1}$ for Co $K\alpha$ radiation and $0.032\ \text{cm}^{-1}$ for Cr $K\alpha$ radiation. The absorption coefficient for Mo $K\alpha$ radiation, $\mu_{\text{air}} = 0.001\ \text{cm}^{-1}$, is only one-tenth of that for Cu $K\alpha$ radiation, so an air-absorption correction is not necessary. Alternatively, the absorption correction may be normalized to the absorption level in the beam centre as

$$p_c(x, y) = p_o(x, y)\exp\left\{\mu_{\text{air}}\left[(D^2 + x^2 + y^2)^{1/2} - D\right]\right\}. \quad (2.5.31)$$

In this normalized correction the attenuation by air scatter is not fully corrected for each pixel, but rather corrected to the same attenuation level as the pixel in the detector centre. This means that the effect of path-length differences between the detector centre pixel and other pixels are eliminated.

2.5.3.3.6. *Sample absorption*

The absorption of X-rays by the sample reduces the diffracted intensity. Many approaches are used to calculate and correct the absorption effect for various sample shapes and geometries [*International Tables for Crystallography* Volume C, Chapter 6.3 (Maslen, 1992); Ross, 1992; Pitschke *et al.*, 1996; Zuev, 2006]. The sample absorption can be measured by the transmission coefficient (also referred to as the absorption factor):

$$A = (1/V) \int_V \exp(-\mu\tau)\, \mathrm{d}V, \tag{2.5.32}$$

where A is the transmission coefficient, μ is the linear absorption coefficient and τ is the total beam path in the sample, which includes the incident-beam path and diffracted-beam path. Fig. 2.5.15(a) shows reflection-mode diffraction with a flat-plate sample. The thickness of the plate is t. z is the distance of the element dV from the sample surface. The normal to the reflection surface is **n**. The incident beam is represented by the unit vector $\mathbf{s}_o$ and the diffracted beam by the unit vector **s**. The transmission coefficient is given as (Maslen, 1992)

$$A = \frac{1 - \exp\{-\mu t[(1/\cos\eta) + (1/\cos\zeta)]\}}{\mu[(\cos\zeta/\cos\eta) + 1]}, \tag{2.5.33}$$

where η is the angle between the incident beam and the normal to the sample surface, and ζ is the angle between the diffracted beam and the sample normal. For two-dimensional X-ray diffraction, there is a single incident-beam direction at a time, but various diffracted-beam directions simultaneously, so

$$\cos\eta = \sin\omega\cos\psi \tag{2.5.34}$$

and

$$\cos\zeta = -\cos 2\theta \sin\omega\cos\psi - \sin 2\theta \sin\gamma\cos\omega\cos\psi - \sin 2\theta\cos\gamma\sin\psi. \tag{2.5.35}$$

The transmission coefficient from equation (2.5.33) contains a length unit, which creates ambiguity if such transmission coefficients are used to correct the intensity pixel-by-pixel. In order to make the relative intensity comparable to the results from Bragg–Brentano geometry, we introduce a new transmission coefficient, which is normalized by the transmission coefficient of the Bragg–Brentano geometry, $A_{\rm BB} = 1/(2\mu)$. This normalized transmission coefficient is also a numerical factor without units. The transmission coefficient with normalization will be denoted by T hereafter in this chapter. The transmission coefficient for reflection-mode diffraction with a flat sample of thickness t is then given as

$$T = A/A_{\rm BB} = \frac{2\cos\eta\big(1 - \exp\{-\mu t[(1/\cos\eta) + (1/\cos\zeta)]\}\big)}{\cos\eta + \cos\zeta}. \tag{2.5.36}$$

For a thick plate or material with a very high linear absorption coefficient, the transmission through the sample thickness is negligible and the above equation becomes

$$T = \frac{2\cos\eta}{\cos\eta + \cos\zeta}. \tag{2.5.37}$$

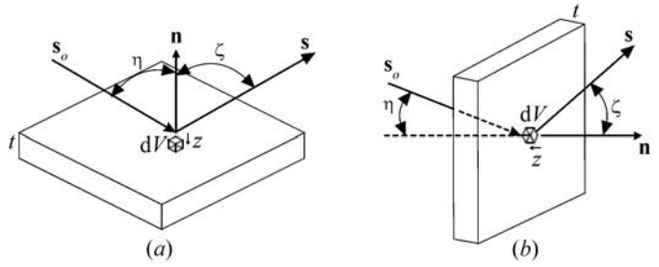

Figure 2.5.15
Absorption correction for a flat slab: (a) reflection; (b) transmission.

Fig. 2.5.15(b) shows transmission-mode diffraction with a flat-plate sample. The thickness of the plate is t. The normal to the reflection surface is represented by the unit vector **n**. The incident beam is represented by the unit vector $\mathbf{s}_o$ and the diffracted beam by the unit vector **s**. η is the angle between the incident beam and the normal of the sample surface, and ζ is the angle between the diffracted beam and the sample normal.

The transmission coefficient normalized by $A_{\rm BB} = 1/(2\mu)$ is given by (Maslen, 1992; Ross, 1992)

$$T = \frac{2\sec\eta[\exp(-\mu t\sec\eta) - \exp(-\mu t\sec\zeta)]}{\sec\zeta - \sec\eta} \quad \text{for } \sec\zeta \neq \sec\eta. \tag{2.5.38}$$

For two-dimensional X-ray diffraction in transmission mode

$$\cos\eta = \sin\omega\sin\psi\sin\varphi + \cos\omega\cos\varphi \tag{2.5.39}$$

and

$$\cos\zeta = (\sin\omega\sin\psi\sin\varphi + \cos\omega\cos\varphi)\cos 2\theta + (\cos\omega\sin\psi\sin\varphi - \sin\omega\cos\varphi)\sin 2\theta\sin\gamma - \cos\psi\sin\varphi\sin 2\theta\cos\gamma. \tag{2.5.40}$$

It is very common practice to set the incident angle perpendicular to the sample surface, *i.e.* $\eta = 0$. For most transmission-mode data collection, equation (2.5.40) becomes

$$T = \frac{2[\exp(-\mu t) - \exp(-\mu t\sec\zeta)]}{\sec\zeta - 1}. \tag{2.5.41}$$

When $\eta = \zeta$, both the numerator and denominator approach zero, and the transmission coefficient should be given by

$$T = 2\mu t\sec\zeta\exp(-\mu t\sec\zeta). \tag{2.5.42}$$

It is common practice to load the sample perpendicular to the incident X-ray beam at the goniometer angles $\omega = \psi = \varphi = 0$. Therefore, $\cos\eta = 1$ and $\cos\zeta = \cos 2\theta$, and the transmission coefficient becomes

$$T = \frac{2\cos 2\theta[\exp(-\mu t) - \exp(-\mu t/\cos 2\theta)]}{1 - \cos 2\theta}. \tag{2.5.43}$$

The maximum scattered intensity occurs when

$$t = \frac{\cos 2\theta\ln\cos 2\theta}{\mu(\cos 2\theta - 1)}. \tag{2.5.44}$$

This equation can be used to select the optimum sample thickness for transmission-mode diffraction. For example, if the measurement 2θ range is between 3 and 50°, the preferred sample thickness should be given by μt = 0.8–1.0.

references